ELSEVIER

Journal of Nuclear Materials 304 (2002) 96–106

journal of nuclear materials

www.elsevier.com/locate/jnucmat

Solubility of hydrogen in Zircaloy-4: irradiation induced increase and thermal recovery

P. Vizcaíno, A.D. Banchik *, J.P. Abriata

Centro Atómico Ezeiza, Centro Atómico Bariloche, Comisión Nacional de Energía Atómica, Libertador 8250, C.P.: 1429, Buenos Aires, Argentina

Received 3 January 2002; accepted 22 May 2002

Abstract

The solid solubility of hydrogen isotopes in neutron irradiated Zircaloy-4 core components removed after 10.3 years in service is studied by differential scanning calorimetry (DSC) in two cooling channels of the Atucha I Heavy Water Power Reactor, Argentina. For irradiated Zircaloy-4 samples containing 150–380 ppm-H_{eq} the temperature for hydride dissolution, $TSSd_{irrad}$, measured during the first DSC run was approximately similar to the reactor operating temperature (260–300 °C) and 50–150 °C lower than the TSSd for unirradiated material. This difference decreases in subsequent DSC runs and a stage of stable $TSSd_{irrad}$ intermediate values is reached. After further isothermal annealings the $TSSd_{irrad}$ values approach asymptotically TSSd. These results may be interpreted by assuming that a fraction of the total hydrogen isotope concentration, which is similar to the concentration that should be present in solid solution in unirradiated Zircaloy-4 at the operating temperature, is in solid solution in the irradiated Zircaloy-4 and the rest is trapped and slowly released from complex irradiation induced defects.

1. Introduction

A great deal of attention is currently given to the possibility of increasing the lifetime of zirconium-based materials used in the core region of nuclear power reactors. One of the limits to the time that a zirconium alloy component can stay in the reactor core is given by its rate of absorption of hydrogen isotopes produced during the corrosion reaction between the alloy and the coolant water. Continued hydrogen absorption might eventually result in the precipitation of zirconium hydride and the consequent mechanical failure of the material. Recent experimental results on the temperature of terminal solid solubility in irradiated material obtained by differential scanning calorimetry (DSC) have shown that this temperature is significantly lower than for the unirradiated material for the same bulk hydrogen isotope concentration [1].

Therefore, the irradiated zirconium alloys could in principle absorb relatively large amounts of hydrogen before the precipitation of zirconium hydride occurs. This phenomenon may have important technological applications since a higher effective hydrogen solubility would delay the nucleation of unwanted hydride blisters in zirconium base components, as pressure tubes, thus increasing their lifetime in service. Moreover, a smaller amount of hydrides would precipitate when the reactor cools after its shut down.

To study further the increase in hydrogen solubility in irradiated zirconium alloys an experimental program was implemented in our laboratory to examine samples obtained from the Zircaloy-4 cooling channels of the Atucha I Heavy Water Power Reactor (HWPR) installed in Argentina. These samples were taken from tubes that had been in service for 10.3 full effective power years (fepy) and studied by means of DSC [2,3]. Using this technique, the temperature of terminal solid

* Corresponding author.
E-mail address: banchik@cae.cnea.gov.ar (A.D. Banchik).

0022-3115/02/$ - see front matter
PII: S0022-3115(02)00883-8

solubility on dissolution (TSSd) can be determined from the discontinuity produced in the heat flow vs time curve during the hydride dissolution. In a similar way, the discontinuity in a cooling process defines the temperature of terminal solid solubility for precipitation (TSSp).

These temperatures differ due to a hysteresis phenomenon, but it is well known that TSSd is closer to the true equilibrium temperature value [1,4–6]. This fact, added to the non-reproducibility of TSSp results on irradiated material made us focus on the dissolution process by measuring the temperature of terminal solubility on dissolution, $TSSd_{irrad}$.

For reference purposes, the TSSd curve for unirradiated Zircaloy-4 was also measured over a wide range of hydrogen concentration.

Present observations confirm the result that neutron irradiation increases hydrogen solid solubility in zirconium alloys [1]. Moreover, these observations add new results relative to the amount of irradiation induced solubility increase and the effect of the thermal treatment in the recovery kinetic of the equilibrium solvus line.

This work is organized as follows: Section 2 describes the calorimetric technique, the equipment, the sample preparation for calorimetry, the measurement procedure and the hydrogen plus deuterium concentration, [H + D]. Section 3 presents the results for unirradiated and irradiated material. The discussion and the conclusions are given in Sections 4 and 5, respectively.

2. Experimental procedures

2.1. Calorimetry of irradiated alloys

In the last four decades several techniques have been used to determine the hydrogen solubility in zirconium alloys [1,4–9]. For the present study the DSC technique has been chosen to study highly irradiated materials. This technique has simplifying advantages with respect to the other methods because it only requires small specimens and, being non-destructive, the sample can be tested several times. The calorimeter used is a heat flux type by Shimadzu, model DSC-60. It has a heating chamber with two crucibles. The sample is placed in one crucible and a reference specimen in the other. The samples are heated (and cooled) by a linear ramp up to a xpreviously selected temperature T_{max}. A Chromel–Constantan an differential thermocouple measures the temperature difference between the sample and the reference.

The temperature axis is calibrated with the fixed points for zinc and indium, while the enthalpy change is calibrated with the latent heat of fusion of these two metals.

If no transformation occurs during the thermal cycle, the heat flow vs time curve follows a continuous curve, called the baseline; but when a transformation such as the melting of a pure metal takes place at a certain temperature, a peak superimposed to the baseline is observed. This peak results from the energy absorbed or released in the phase transformation, and its position gives a characteristic temperature for the transition.

In the Zr–H system the dissolution of the zirconium hydrides takes place along a wide temperature range and no sharp peak is observed during the hydride dissolution process. In this case the heat flow curve gradually deviates from the baseline as the temperature increases because part of the heat absorbed is used to increase the hydride fraction dissolved.

During the heating stage the heat flow vs time curve is given by ABMCD, as shown in Fig. 1. At point A the run starts and the temperature reaches T_{max} at point D. After many DSC runs made without any sample, or with two reference samples with equal [H] concentration, the baseline was identified as the curve ABCD, where the dotted segment BC was drawn following the tendency of the segments AB and CD. *The deviation from the BC segment, BMC, is related with the heat absorbed during the hydride dissolution*. At point B a slight change in the heat flow tendency can be seen, where the hydride dissolution starts to be detected. At point C the dissolution process finishes, and this point is called the completion, as can be seen in Fig. 1. The change observed after point

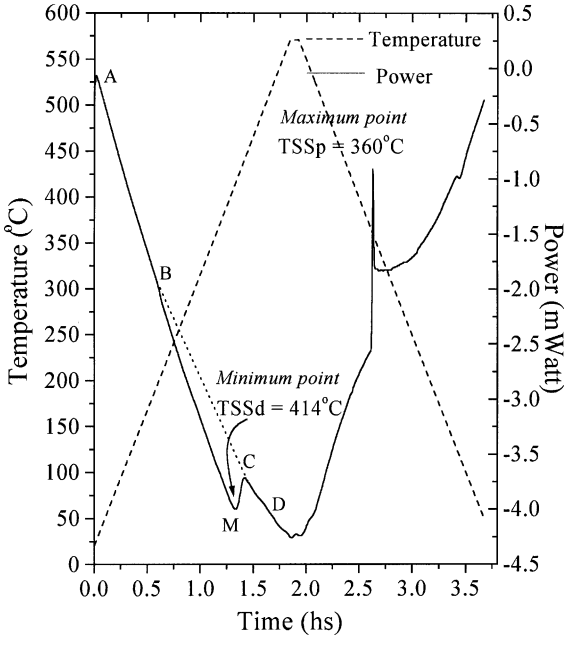

Fig. 1. Temperature/heat flow-time curves for a fully recrystallized Zircaloy-4 sample with 270 hydrogen ppm. Heated at a rate of 5 °C/min to T_{max} = 570 °C and then cooled at the same rate.

M, i.e. segment MC, can be used to determine the temperature of terminal solid solubility on dissolution, TSSd. After a short plateau at T_{max} (550 °C), the cooling starts and we can see a sharp peak on the baseline, which indicates the onset of the precipitation. The peak is related with the temperature of terminal solid solubility on precipitation, TSSp, and can be used to determine this temperature.

Even though the peaks are related to the dissolution and precipitation processes, there are no established rules for choosing the point in the peak that can be identified with TSSd and TSSp. In the idealized case the hydride dissolution is indicated by a sharp discontinuity, and there is no doubt that the temperature of terminal solid solubility is related to this peak. However, due to the calorimeter response and hydride dissolution behavior the change from M to C is not sharp. Thus, in the hydride dissolution three points are generally related with TSSd along MC: the minimum, the completion and the position of an inflection point between the completion and the minimum.

Some authors identify the minimum with TSSd and, with a similar criterion, the sharp peak in the cooling stage as TSSp. Others choose the completion point C, defined by the intersection of the tangent to the upraised side of the curve and the baseline as the end for the dissolution. Similar criteria are applied for TSSp. These temperatures are called completion temperatures. Some others, such as McMinn et al. determine these two temperatures calculating the derivative of the heat flow curve. They take the extreme values corresponding to the inflexion points of the heat flow curve [1]. These temperatures are also called maximum slope temperatures.

In the present work the temperature for the minimum (point M) is chosen as TSSd. This choice is based on the fact that the minimum gives the more reproducible and reliable data for the irradiated material. In the irradiated material, the heat flow curve in the first run often presents some noise possibly due to the highly unstable condition of the material. The derivative of the heat flow curve amplifies this noise and consequently does not produce sharp peaks. Thus, the maximum slope temperature sometimes is not a reliable value. The same can be applied to the completion temperature because this criterion requires good baseline extrapolations of the BC segment. Hence, the choice of the minimum to determine TSSd avoids mathematical subjectivity. In addition it must be pointed out that the choice of any of the three criteria does not affect the conclusions because they are based on the evolution of the TSSd and not on its absolute value. Furthermore, the data obtained for unirradiated Zircaloy-4 using the criteria mentioned above are in good agreement with the Kearns equilibrium data, a classical reference, in the range of hydrogen concentrations that was considered [2,3,10].

2.2. Materials

The samples for TSS measurements were cut from two cooling channels removed after 10.3 fepy of operation, one channel from the center of the core and the other from the outer layer of the (HWPR) of Atucha-1 Nuclear Power Station (NPS). The core of this power station is made up of 276 vertical cooling channels where the fuel elements are installed. The cooling channels are made of Zircaloy-4 satisfying ASTM B-352, with a fully recrystallized microstructure and a grain size of 19 ± 6 μm. Their chemical composition is given in Table 1.

The nominal temperature profile of the cooling channels is the same for both channels, 263 °C at the bottom and 303 °C at the top. The flux distribution for fast neutrons ($E > 1$ MeV) depends on both the axial and radial directions in the core. It reaches its maximum value at the center of the core, and decreases along the radial direction. Lerner and Fink calculated the neutron flux profile using the PUMA code [11]. The neutron fluency values calculated for 10.3 fepy at selected axial positions are shown in Tables 2 and 3 [11]. Samples from both cooling channels were studied, eighteen from Regions 1–4 of the central channel (CC), and five from Region 3 of the outer channel (OC). Regions 2–4 were taken from the active length of the channels and Region 1 from the outside of the active length.

During operation, the core Zircaloy-4 components absorb deuterium from the heavy water coolant. Thus, the total hydrogen isotope concentration, [H + D], is the sum of the hydrogen concentration of the original material in the 'as fabricated' condition, and the amount of deuterium that was incorporated into the metal during operation. The [H + D] of the samples were measured with a LECO RH-1 hydrogen meter. As the sensitivity of the hydrogen analyzer depends on the thermal conductivity of the gas that is analyzed, a calibration was done on isotopic effects to obtain a correction factor for deuterium using deuterium gas instead of hydrogen. The final [H + D] values were calculated assuming that the material from both channels has an 'as fabricated' concentration of 20-ppm with a dispersion minor to 5 ppm. The [H + D] measurements are presented as hydrogen equivalent in ppm by weight, which is defined as

Table 1
Zircaloy-4 composition (wt%) obtained by chemical analysis[a]

Channels	Alloying elements (wt%)			
	Sn	Fe	Cr	Ni
Central	1.6	0.22	0.065	0.0032
Outer	1.6	0.21	0.07	0.0041

[a] The chemical analysis was made with an atomic absorption equipment with a Shimadzu graphite furnace by the chemical laboratory of the Nuclear Power Plant CNA-1, Argentina.

Table 2
Estimated fluences, [H + D], TSSd values from Eq. (1), $TSSd_{irrad}$ values for the first three runs, stable zone and after annealing. The last two columns show the differences between post-annealing values and first run values and between TSSd (Eq. (1)) and post-annealing values

Region	Sample	fluence ($\times 10^{22}$ n/cm^2)	T_{op} (°C)	[H + D] (ppm-H_{eq})	TSSd (°C)	$TSSd_{irrad}$ (°C)						ΔTSSd (°C)	
						First run	Second run	Third run	Stable	After 2 h at		Post-anneal-first run	TSSd-Post-anneal
										508 °C	611 °C		
3 OC	1	0.42	280	237	401	275	344	348	373	376	–	101	25
	2			156	363	250	316	315	331	337	–	87	26
	3			225	396	268	292	318	–	364	–	96	32
1 CC	1	<0.05	263	179	375	288	295	296	303	–	345	58	30
	2			185	378	279	282	302	304	–	351	72	27
	3			191	381	297	303	304	307	–	356	59	25
2 CC	1	0.70	268	157	363	264	275	277	292	295	–	31	68
	2			159	365	257	268	278	292	298	–	41	67
	3			174	373	260	278	281	300	300	–	40	73
3CC	1	1.00	280	156	363	277	307	311	315	–	328	51	35
	2			179	375	316	316	325	328	–	344	28	31
	3			157	363	289	309	308	316	–	326	37	37
	4			157	363	289	306	317	316	–	331	42	32
	5			163	367	285	318	320	321	–	334	49	33
	6			169	370	291	314	309	310	–	324	33	46
	7			181	377	291	310	311	311	–	322	31	55
4CC	1	0.90	298	211	390	327	339	340	–	354	–	27	36
	2			260	410	324	328	330	–	344	–	20	66
	3			250	406	326	326	339	–	352	–	26	54

Table 3
Estimated fluences, [H + D], TSSd values from Eq. (1), $TSSd_{irrad}$ values for the first run, annealing temperatures, TSSd values measured after annealing, and, in the last two columns, the differences between the post-annealing value and first run values, and between TSSd from Eq. (1) and post-annealing values

Region	Sample	Fluence ($\times 10^{22}$ n/cm^2)	T_{op} (°C)	[H + D] (ppm-H_{eq})	TSSd (°C)	$TSSd_{irrad}$ (°C) First run	$T_{annealing}$ (°C)	Annealing times (h)	TSSd (°C) Post-anneal	ΔTSSd (°C)	
										Post-anneal-first	TSSd-Post-anneal
2 CC	A	0.70	268	178	375	246	508	2	301	55	
							611	12	328	82	47
	B			220	394	258	611	83	366	108	28
3 OC	C	0.42	280	181	376	258	380	32	343	85	
							410	32	343	85	
							700	1	351	92	25
	D		381	450	265	380	32	347	82		
							611	83	439	174	
							700	1	446	181	4

the hydrogen original content by weight (20 ppm) plus half the deuterium content by weight [12]. The global error of the [H + D] determination is estimated in 10 ppm. In addition it should be pointed out that the results obtained for the seven samples from Region 3 CC prove the good reproducibility of the process, where the statistical error is of 4 ppm.

2.3. Sample preparation for calorimetry

Samples of regular form weighing between 50 and 130 mg were cut with a diamond disc cutter from rings taken from Regions 1, 2, 3 and 4 of the CC and Region 3 of the OC. The edges were rounded off with SiC paper and the samples were then chemically pickled with a solution made up of water (50%), HNO_3 (40%) and HF (10%) to remove scale fragments and improve surface smoothness. Finally, the samples were washed with water and dried out with acetone and hot air.

2.4. Measurement procedure

A piece of unirradiated recrystallized Zircaloy-4 with a hydrogen content of 20 ± 5 ppm was used to make the reference specimens. For each sample the weight of the reference specimen was reduced until the difference in weight with the sample was less than 1 mg.

In a previous work we proved that the effect of the heating rate is negligible in the range of 5–30 °C/min [2]. Exploratory runs in irradiated material have shown that the definition of the dissolution peaks depends on the heating rate. Thus, some samples were tested in the range of 5–50 °C/min to choose the most convenient rate. The dissolution peak was not observed at low rates such as 5 °C/min and was not well-defined at 10 °C/min. The definition improves at 15 °C/min and heating rates higher than 20 °C/min produced a well-defined minimum. Because high heating rates do not ensure thermal homogeneity on the samples, a rate of 20 °C/min was chosen as the best balance between peak definition and thermal homogeneity.

The TSSd determinations were made using the software associated with the DSC equipment and the experimental error is estimated to be of the order of ±1 °C.

The measurements were made in series, each with a specific sequence of operations. The series include several thermal runs to a T_{max} at constant heating rate with no holding time at T_{max}. The value of T_{max} was 380 °C and it was selected taking into account the [H + D] range of the samples. As a result, part of the thermal cycle is made at temperatures above the operating temperature of the reactor (263–303 °C), T_{op}. The samples were then annealed for about 10 min at temperatures between T_{op} and T_{max} in each run.

After the runs to T_{max}, a 2 h isothermal annealing at a $T_{annealing}$ of 508 or 611 °C was done. Finally a few ad-

ditional runs were made to determine the TSSd post annealing value and check stability.

Subsequently new series were made with another lot of four samples at isothermal conditions for different periods of time, and TSSd was measured between each one.

The [H + D] analysis of each irradiated sample was made after the calorimetric measurements.

3. Results

3.1. Unirradiated samples

The terminal solid solubility of hydrogen of unirradiated and fully recrystallized Zircaloy-4 was determined, and the experimental values of hydrogen concentration vs TSSd were fitted to an exponential curve [2,3]. The parameters that minimized the error in the fit are given in Eq. (1):

$$C_{\mathrm{Tssd}}(T) = 263\,024\mathrm{e}^{-4728/\mathrm{T}}\ \text{ppm}. \quad (1)$$

Fig. 2 shows the fit to the experimental points. Fig. 2 also includes the curves calculated using the equation given by McMinn et al. [1] and by Kearns [10].

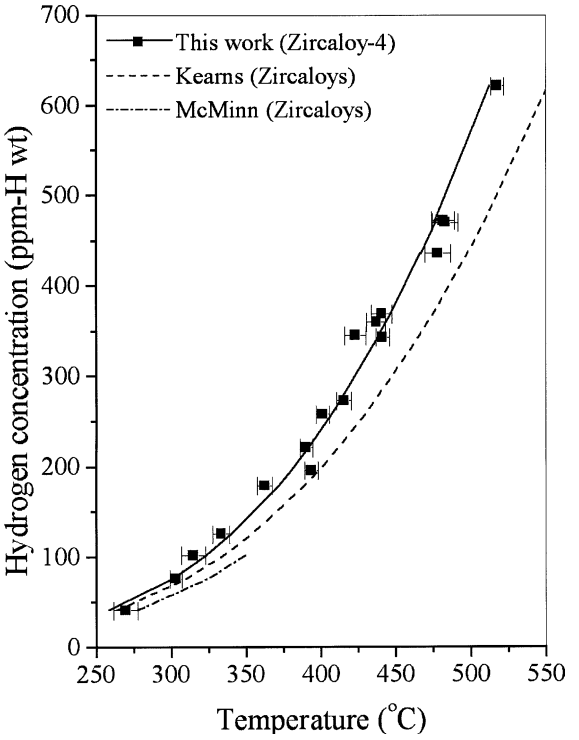

Fig. 2. Hydrogen concentration vs TSSd values. The solid curve fits the unirradiated Zircaloy-4 data (Eq. (1)). The dotted and dash-dotted lines correspond to the curves of Kearns [10] and McMinn et al. [1].

McMinn's results were for Zircaloy-4 specimens with different microstructures and in a hydrogen concentration range of 20–80 ppm using the calorimetric technique. Kearns determined the terminal solid solubility in Zircaloy-4 from a hydrogen analysis of the low-concentration part of diffusion couples, a quasi-equilibrium method, in a wider hydrogen concentration range of 40–650 ppm.

3.2. Irradiated samples

The calorimetric data for the irradiated material are shown in Tables 2 and 3. Table 2 shows the $\mathrm{TSSd_{irrad}}$ data for the irradiated material that were taken from the five regions of the two cooling channels. In addition, the estimated fluences and operating temperatures, the [H + D] values and TSSd values calculated from Eq. (1) are included.

As can be seen from Table 2, after a few runs the largest increase in the $\mathrm{TSSd_{irrad}}$ values are observed for Region 3 OC. During subsequent runs the $\mathrm{TSSd_{irrad}}$ values increase slowly but remain 30 °C below the expected unirradiated value. The annealing at 508 °C *does not* produce any significant change, as shown by Fig. 3. Smaller increases are observed after the first runs in samples from Regions 2 and 4 CC in Fig. 4. Again the annealing at 508 °C for 2 h failed to increase the $\mathrm{TSSd_{irrad}}$ values. The differences between the post-annealing and the unirradiated values for Region 2 are on average about 70 °C and about 60 °C, for Region 4.

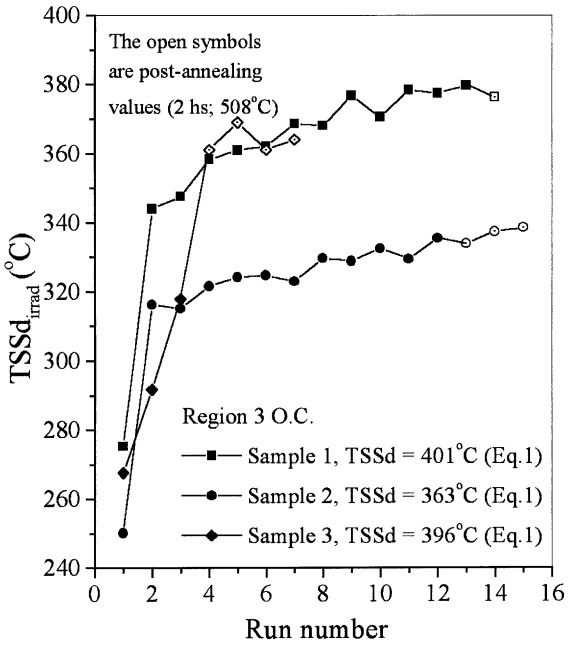

Fig. 3. Evolution of $\mathrm{TSSd_{irrad}}$ with runs for the samples of Region 3 OC annealed at 508 °C for 2 h.

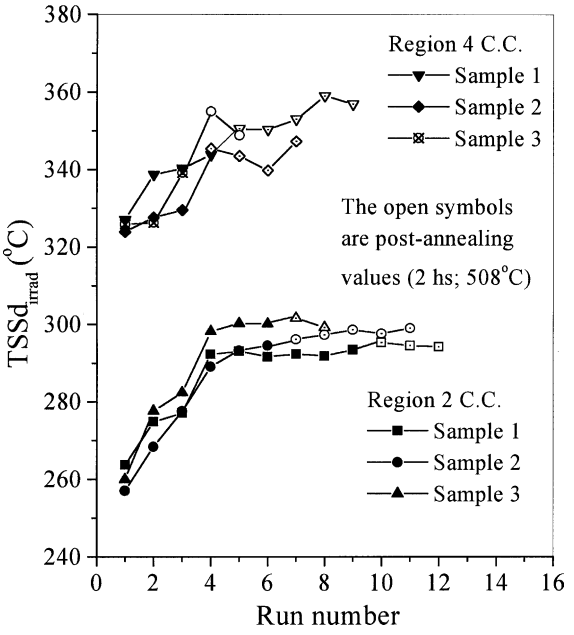

Fig. 4. Evolution of $TSSd_{irrad}$ for the samples of Regions 2 and 4 CC annealed at 508 °C for 2 h.

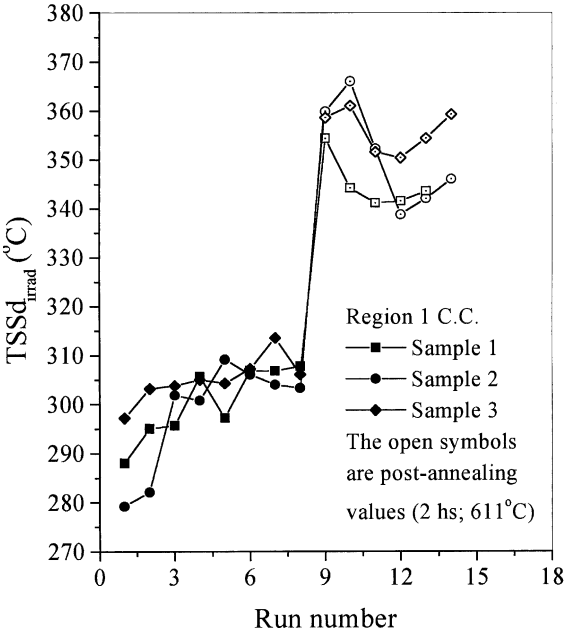

Fig. 5. Evolution of $TSSd_{irrad}$ with runs for the three samples of Region 1 CC annealed at 611 °C for 2 h.

The samples from Regions 1 and 3 CC were annealed at 611 °C. Region 1 CC was out of the active zone and its fluence is estimated to be at least one order of magnitude smaller than for the rest of the regions. These samples show the lowest $TSSd_{irrad}$ increase after the first few runs, as can be seen in columns 6–9 of Table 2, and the largest increase, of about 50 °C, after 2 h at 611 °C, as shown in Fig. 5. However, the post-annealing $TSSd_{irrad}$ values were still 30 °C below the unirradiated TSSd value.

Samples from Region 3 CC follow the same trend as samples from Regions 3 OC and 2 and 4 CC. The increase in $TSSd_{irrad}$ values is significant during the first runs, after which $TSSd_{irrad}$ tends to stabilize. Annealing at 611 °C for 2 h increases the $TSSd_{irrad}$ values of the different samples by about 15 °C, but the post-annealing $TSSd_{irrad}$ values are still far from the unirradiated TSSd. In addition, the seven samples from this region show that the reproducibility of the measurements is good, as can be seen from Table 2, Columns 6–9.

The above results indicate that thermal annealing at higher temperatures and longer periods of time at $T_{annealing}$ are needed to reach the unirradiated TSSd values. The results for four samples subjected to special thermal annealings are given in Table 3.

Sample A was cut from the Region 3 CC and after six runs to 380 °C it was isothermally annealed 2 h at 508 °C and then 12 h at 611 °C with the aim of reaching the TSSd unirradiated value. The six runs to 380 °C produce an increase in $TSSd_{irrad}$ of 30 °C, from 246 to 280 °C.

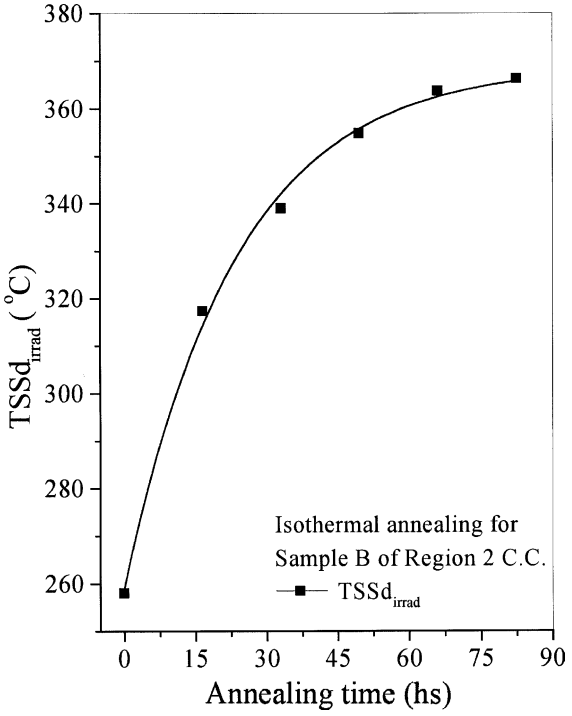

Fig. 6. Effect of isothermal annealing at 611 °C in periods of 16.5 h on the $TSSd_{irrad}$ values for Sample B, Region 2 CC.

The annealings at 508 °C were made in two stages of 1 h. After the first stage $TSSd_{irrad}$ increases 15 °C up to 296 °C, the second stage has a small effect, increasing it to 301 °C. The annealing at 611 °C was also divided in two stages, the first of 2 h and the second of 10 h. The first has a small effect on $TSSd_{irrad}$, increasing it to 308 °C, but the second has a strong effect increasing $TSSd_{irrad}$ to 328 °C. This value is still 48 °C below the unirradiated TSSd value. Thus, longer annealing times were applied.

For instance, Sample B was subjected to a unique thermal treatment at 611 °C made up of five cycles of 16 h each. The $TSSd_{irrad}$ values were measured during the heating-up ramp of each cycle, as can be seen in Fig. 6. The values follow a sigmoidal type curve that gradually increases towards an equilibrium value with smaller increases after each annealing time. However, after 83 h at 611 °C the final $TSSd_{irrad}$ value is still 28 °C below the unirradiated TSSd.

Sample C was subjected to a sequence of three isothermal annealing. The first at 380 °C for 32 h, the second for at 410 °C for 32 h and the third at 700 °C for 1 h. After the first annealing $TSSd_{irrad}$ is 85 °C higher than the initial value and 33 °C below the unirradiated value. After annealing at 410 °C TSSd does not change and after annealing at 700 °C for 1 h the difference between the two last $TSSd_{irrad}$ values is only a few degrees and still remains 25 °C below the unirradiated value.

Even though the [H + D] concentration of the sample D is nearly twice the [H + D] of sample C, $TSSd_{irrad}$ for the first run is in the range of the rest of the samples. After a few runs $TSSd_{irrad}$ reaches stable values and after 32 h at 380 °C $TSSd_{irrad}$ maintains stable temperature. The subsequent long annealing at 611 °C for 83 h increases $TSSd_{irrad}$ by 174 °C. Again, the annealing at 700 °C for 1 h does not produce a significant change in $TSSd_{irrad}$. However, sample D is the only one where the unirradiated value was nearly reached. The dotted line observed in Fig. 7 is the unirradiated value calculated with Eq. (1) for a material with 381 ppm of hydrogen.

In summary, the results indicate that $TSSd_{irrad}$ increases rapidly during initial runs, and stabilizes after the fourth run. The annealings for 2 h had little effect at 508 °C and a significant effect at 611 °C, but the TSSd expected for unirradiated material was not reached. The long isothermal annealings at 611 °C show that $TSSd_{irrad}$ slowly approaches the unirradiated value.

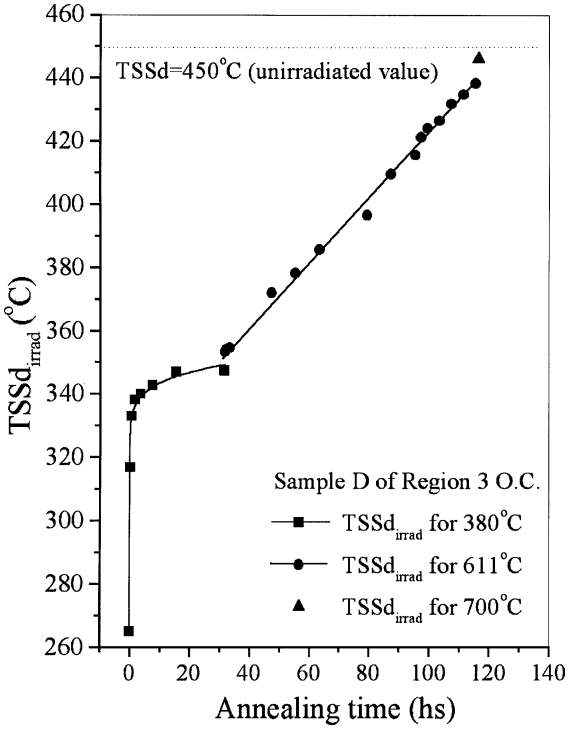

Fig. 7. Effect of isothermal annealings at 380 °C (32 h), 611 °C (83 h) and 700 °C (1 h) on $TSSd_{irrad}$ for Sample D of Region 3 OC.

4. Discussion

4.1. Unirradiated material

The unirradiated Zircaloy-4 results shown in Fig. 2 are on average 15–20 °C higher than those of McMinn et al., who also used the DSC technique to measure TSSd. It is believed that the differences arise from the different criteria used to identify TSSd value. In the present work, the TSSd values have been determined from the minimum in the dissolution peak of the heat flow vs time curve, while McMinn et al. have chosen the maximum slope temperature as the TSSd temperature. The maximum slope temperature is higher than the peak temperature by nearly 20 °C on average. If the differences in criteria are taken into account, both results coincide within experimental error. On the other hand, Kearns determined the terminal solid solubility in Zircaloy-4 specimens with complex microstructures. Kearns used welded diffusion couples, a quasi equilibrium method, to determine TSS. The range of hydrogen concentrations in Kearns' work was larger than the range used in the present work. Fig. 2 shows that the curves given here and by Kearns are similar in shape, but they tend to diverge at concentrations higher than 250 ppm of hydrogen. However, in the present work, the differences with Kearns are still irrelevant, since the [H + D] concentration range of the irradiated samples is between 150 and 260 ppm, with the exception of a sample of 380 ppm. From now on Eq. (1) is used as the reference to make comparisons with the results corresponding to irradiated material.

4.2. Irradiated material

The most significant result obtained on irradiated material is the observation that neutron irradiation increases hydrogen solubility. As can be seen from Tables 2 and 3 $TSSd_{irrad}$ values for the first run are on average 100 °C lower than the expected unirradiated value. This behavior was systematically observed in all the samples analyzed.

The runs subsequent to the first one have a strong effect on $TSSd_{irrad}$, increasing its values by 60 °C on average. This effect decreases after the fourth run and $TSSd_{irrad}$ reaches a stable value. Figs. 3–5 clearly show this behavior. The sequence of isothermal annealings made at 380 °C (samples C, D and Fig. 7) shows a similar behavior and reaches a stabilized zone as observed after multiple runs. Again TSSd was considerably below the expected unirradiated values.

Isothermal annealings at higher temperatures, such as 508 and 611 °C, were necessary to continue the evolution of TSSd toward the unirradiated values. Annealings of 2 h at 611 °C increased $TSSd_{irrad}$ values. However, after the annealing values were still 30–40 °C below unirradiated values, as shown in Table 2. Longer isothermal annealings to this temperature were needed to make $TSSd_{irrad}$ closer to the unirradiated values, and this was only reached in one case (see Table 3, Sample D).

The above results suggest that the evolution of TSSd for irradiated material can be divided into three stages. A first stage, where the runs have a significant effect on $TSSd_{irrad}$, a second stage, where $TSSd_{irrad}$ reaches a stable value which is not affected by further runs to T_{max}, and a third one, where the solubility gradually approaches that of the unirradiated material after long isothermal annealings at higher temperatures.

The results of the present work differ from McMinn's results in two respects: $TSSd_{irrad}$ values for the first run are considered here as part of the data while McMinn discards these first values, after which the same experimental procedure is followed. Another difference arises from the temperatures and times involved in the recovery, which are quite different. While in McMinn the recovery is complete or fairly complete with isothermal annealings of 1 h at 500 °C, in the present work longer annealings at higher temperatures were needed, i.e. 80 h at 611 °C, to get TSSd values similar to the unirradiated one.

It is clear that the most representative value of TSSd for the material in the core reactor conditions corresponds to the first run because the minimum, shown in Fig. 1, is observed during the heating ramp in the operating temperature range without any previous thermal treatment.

There exist differences in the materials used in both works, which can contribute to explain the discrepancies. The irradiated Zircaloy-4 samples used for the present work were hydrided (deuterided) during the operating time in the reactor core, which lasted for more than 10 years. With the exception of the samples from the Zircaloy-2 pressure tube, McMinn hydrided the pre-irradiated samples by diffusion annealing at 260 °C outside the reactor. Thus, the hydride formation occurs in a different condition and by a different process. Furthermore, it should be noted that this annealing temperature is slightly below the average value of $TSSd_{irrad}$ first run values of the present work. Hence, an effect of the annealing temperature on the $TSSd_{irrad}$ should not be excluded from the McMinn data.

To explain the present results it should be first pointed out that if the material behaves as unirradiated Zircaloy-4 with a [H + D] of about 150–260 ppm, all the $TSSd_{irrad}$ values for the first run should be much higher than the observed values. Assuming that the terminal solid solubility of irradiated material is given by Eq. (1), these $TSSd_{irrad}$ first run values would be compatible with a concentration range of 40–70 ppm of hydrogen.

As was shown, in the irradiated material with a bulk concentration ranging from 150 to 360 ppm the experimental $TSSd_{irrad}$ values are close to the reactor operating temperature, T_{op}, as shown in Fig. 8. If it is assumed as a

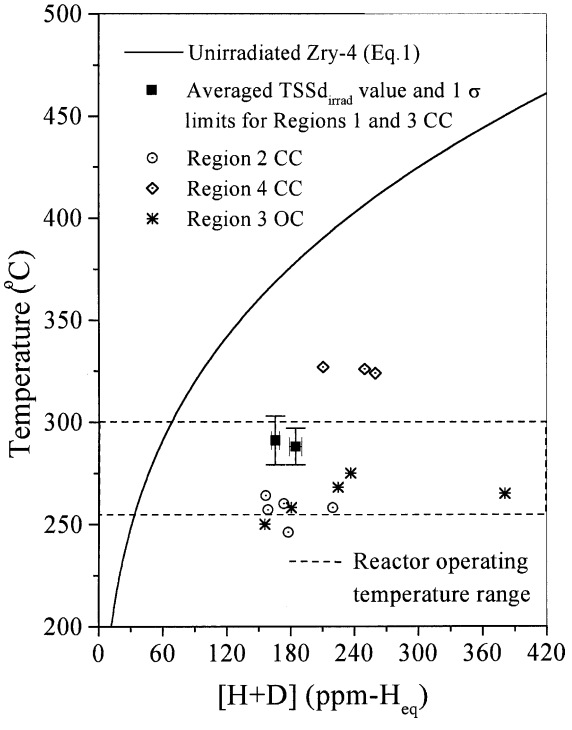

Fig. 8. $TSSd_{irrad}$ first run values for Regions 2 CC, 4 CC and 3 OC and averaged $TSSd_{irrad}$ values for Regions 1 and 3 CC vs [H + D]. The solid line corresponds to unirradiated fully recrystallized Zircaloy-4 (Eq. (1)).

first approximation that $TSSd_{irrad} \approx T_{op}$, only the fraction of the bulk concentration predicted by Eq. (1) will be in solid solution at T_{op}. The rest of the atoms will be in a metallurgical condition to be explained.

A hypothesis compatible with the effect of the thermal annealing on the evolution of $TSSd_{irrad}$ seems to be the irradiation defect trapping mechanism. This hypothesis assumes that there exists an interaction between the defects and the hydrogen isotope atoms which tend to trap the atoms at the defects [1,13]. This hypothesis could be applied to the present result as follows. As the bulk [H + D] grows, the solid solution concentration increases until it reaches the solubility limit at the operating temperature in 3–4 years. After crossing the solubility limit the atoms in excess to the amount corresponding to the solubility limit at the operating temperature will be trapped by irradiation defects that were produced by the neutron flux during the previous years of operation. When the reactor is shut down and the core cooled, only the atoms in solid solution precipitate as hydrides because the trapped atoms remain in their traps. This assumption is based on the similarity between $TSSd_{irrad}$ for the first run and T_{op}. However the $TSSd_{irrad}$ value for Region 4 CC is 25 °C above the maximum T_{op}. Hence, at the upper limit of the operating temperature range a certain amount of hydrides could be present at about 300 °C, but the amount would be smaller than the value predicted by Eq. (1).

Finally, the trapping hypothesis can also explain the $TSSd_{irrad}$ evolution with the thermal annealings by assuming that the DSC runs and the isothermal annealings gradually release the hydrogen isotope atoms from their traps. Assuming that the amount of trapped atoms reaches a stable value after the long period at T_{op}, it is reasonable to think that at temperatures lower than T_{op} no atoms are released during the DSC runs. Moreover, the rest of the cycle from T_{op} to 380 °C and then back to T_{op} has an annealing effect on the radiation damage, and this annealing releases successively the hydrogen atoms from their traps until the stable zone is reached. The behavior of Samples C and D of Region 3 OC during the long isothermal annealing at 380 and 410 °C reinforces the hypothesis of a stable stage with no release of atoms (see for example Fig. 7).

The release of the hydrogen isotope atoms from the traps can be attributed to the recovery of the radiation damage. The temperature range at which the damage is annealed can be related to that of the recovery of the mechanical properties. Data in the literature show that the onset of hardness recovery of zirconium alloys starts at 300 °C and ends at 460 °C [14]. For example, Zircaloy-2 irradiated at a fast neutron fluence of 5.5×10^{19} n/cm^2 showed a 50% recovery in hardness at 380 °C [14]. The yield strength of annealed Zircaloy-2 irradiated at 2.7×10^{20} n/cm^2 was almost completely recovered between 300 and 400 °C [15].

At temperatures around 300 °C there is a high mobility of point defects, vacancies and interstitial atoms, all of which migrate to the grain boundaries where they are absorbed, or to interstitial loops [16]. In a recent work it has been suggested that $\langle a \rangle$ component dislocation loops play a significant role in hydrogen trapping [1]. These data can explain the observed behavior in all the analyzed cases for the first and second stages by assuming that the annihilation of the $\langle a \rangle$ loops during the runs to T_{max} releases a fraction of the trapped atoms. In addition the great increase in $TSSd_{irrad}$ observed for the low fluence samples of Region 1CC after the annealing at 611 °C may be related to the $\langle a \rangle$ loops annihilation.

However, a second trapping mechanism is necessary to explain the evolution of $TSSd_{irrad}$ in the third stage for the high fluence samples. The difficulty to reach the equilibrium values for all the samples with a high neutron fluence is attributed to the stability of the $\langle c \rangle$ component dislocation loops, which remain as traps for hydrogen isotope atoms after annealing [1,17].

This fact is in agreement with the small or null effect of the annealing at 508 °C. It is also reinforced by the long annealings at 611 and 700 °C needed to reach the unirradiated values, suggesting that the release of atoms is related with the dissolution of $\langle c \rangle$ type dislocation loops.

The hydrogen-trapping mechanism seems to be a good hypothesis to explain the results, but it should be pointed out that it is still difficult to believe that the dislocation loops need such long periods of time at 600 or 700 °C to be annihilated. In addition, the large difference in temperature and time to release the atoms during the first two stages and the final one implies that the trapping mechanism, which acts at the first two stages, has a binding energy much lower than the last one. Thus, it would be reasonable to propose another type of trap.

It is possible that an interaction between the hydrogen isotope atoms and other solute atoms or second phase precipitates be responsible for the third stage. For instance, it is well known that second phase precipitates as $Zr(Fe_x, Cr_{1-x})_2$ have a high capacity to absorb hydrogen and its capacity increases when x decreases [18]. In addition it has been shown that the irradiation releases iron atoms from the precipitates [19], then, the decrease of iron concentration in this precipitates could provide another type of trapping mechanism.

From a technological point of view, the fact that $TSSd_{irrad}$ is much lower that TSSd implies that zirconium core components can absorb more hydrogen isotope atoms before the hydrides precipitate.

5. Conclusions

Zircaloy-4 samples have been obtained from different positions along two cooling channels, central and outer,

removed from the core of the HWPR Atucha I power plant in Argentina after 10.3 full effective power years. These samples have been studied using the DSC technique to determine the effects of neutron irradiation on the terminal solid solubility of [H + D] in Zircaloy-4. For comparison with previous results as well as for reference purposes, the solubility of hydrogen in unirradiated Zircaloy-4 has also been measured in the range 40–630 ppm.

For the irradiated material, the $TSSd_{irrad}$ values obtained during the first DSC run are much lower than the corresponding TSSd values in unirradiated Zircaloy-4 for the same [H + D] content. In addition, these initial $TSSd_{irrad}$ values are fairly close to the reactor operating temperatures. After a few additional DSC runs, $TSSd_{irrad}$ reaches a stable value but at temperatures systematically lower than those corresponding to unirradiated Zircaloy-4. Additional thermal treatments at temperatures of 500 °C and higher increases further $TSSd_{irrad}$ which asymptotically tends to TSSd. However, only after isothermal annealing for 83 h at 611 °C and 1 h at 700 °C was it possible to reach the TSSd value for the corresponding [H] concentration.

As all the initial $TSSd_{irrad}$ values are around the reactor operating temperature range, it is predicted that under reactor operation conditions the fraction of hydrogen atoms in excess with respect to the zirconium alpha phase solid solubility are trapped by complex irradiation induced defects. The increase in $TSSd_{irrad}$ values with the thermal treatments could then be attributed to the gradual release of hydrogen/deuterium atoms from these defects. However, the final steps of the recovery kinetics are difficult to understand, and the possibility of solutes and second phase particles in Zircaloy-4 interacting with the hydrogen isotope atoms cannot be excluded.

Acknowledgements

The authors are grateful to Professor Clement Lemaignan for his comments and suggestions, to Ruben Ríos for the hydrogen plus deuterium measurements and the preparation of the solutions for the chemical analysis of the irradiated samples. Furthermore, the authors are indebted to Ricardo Manzi and Oscar Iglesias from the Chemical Department of Atucha 1 Nuclear Power Plant for the chemical analysis of the irradiated samples.

References

[1] A. McMinn, E.C. Darby, J.S. Schofield, Zirconium in the nuclear industry, in: Twelfth International Symposium, Toronto, 15–18 June 1998, ASTM STP1354, American Society for Testing Material, Philadelphia, PA, 2000.
[2] P. Vizcaíno, A.D. Banchik, Materia, 3, No. 2, 1999. Available from http://www.materia.coppe.ufrj.br/anteriores/32.
[3] P. Vizcaíno, A.D. Banchik, Proceeding, Symposium Materia 2000. Rio de Janeiro, 23–27 October 2000. Available from http://www.sm2000.coppe.ufrj.br/revisados/vizcaino@cae.cnea.gov.ar_1.doc.
[4] Z.L. Pan, I.G. Ritchie, M.P. Puls, J. Nucl. Mater. 228 (1996) 227.
[5] I.G. Ritchie, Z.L. Pan, Philos. Mag. A 63 (1991) 1105.
[6] D. Khatamian, V.C. Ling, J. Alloys Comp. 253&254 (1997) 162.
[7] G.F. Slattery, J. Inst. Met. 95 (1967) 43.
[8] W.H. Erickson, D. Hardie, J. Nucl. Mater. 13 (1964) 254.
[9] R.W.L. Fong, S. Spooner, Scrip. Met. Mater. 30 (1994) 649.
[10] J.J. Kearns, J. Nucl. Mater. 22 (1967) 292.
[11] C. Grant, PUMA System, Version 4 for Windows, Argentine Nuclear Atomic Energy, Avenida del Libertador 8250, Buenos Aires, Technical Internal Report, CNEA.C.RCN.MUS-034, 1999.
[12] A.D. Banchik, R. Ríos, D. Bianchi, Proceeding of 7th General Conference on Nuclear Energy, Minascentro, Belo Horizonte, MG, Brazil, 27–30 October 1998.
[13] M.B. Lewis, J. Nucl. Mater. 125 (1984) 152.
[14] G.J.C. Carpenter, J.F. Watters, Zirconium in nuclear applications, ASTM STP 551, 21–24 August 1973, American Society for Testing Materials, Portland, WA, 1974.
[15] L.M. Howe, W.R. Thomas, J. Nucl. Mater. 2 (1960) 248.
[16] M.S. Anand, W. Mansel, G. Wallner, W. Weck, J. Nucl. Mater. 126 (1984) 144.
[17] M. Griffiths, R.A. Holt, A. Rogerson, J. Nucl. Mater. 225 (1995) 245.
[18] D. Shaltiel, I. Jacob, D. Davidov, J. Less-Common Met. 53 (1977) 117.
[19] F. Lefebvre, C. Lemaignan, J. Nucl. Mater. 171 (1990) 223.